JOURNAL OF THEORETICAL AND APPLIED MECHANICS
50, 3, pp. 681-699, Warsaw 2012
50th Anniversary of JTAM

A COMPUTATIONAL PROCEDURE FOR THE DYNAMIC ANALYSIS OF THE CATENARY-PANTOGRAPH INTERACTION IN HIGH-SPEED TRAINS

Jorge Ambrósio, João Pombo, Manuel Pereira, Pedro Antunes, António Mósca
IDMEC – Instituto Superior Técnico, Universidade Técnica de Lisboa, Lisboa, Portugal
e-mail: jorge@dem.ist.utl.pt; jpombo@dem.ist.utl.pt; mpereira@dem.ist.utl.pt

The quality of the current collection of high-speed trains is dependent on the compatibility of the catenary and pantograph dynamics and on its implications on the contact force. The design and analysis of these systems using proper computational procedures allows capturing all the relevant features of their dynamic behavior. This work proposes an approach to the dynamics of the energy collection system based on the finite elements method, for the catenary, and on multibody dynamics methods, for the pantograph, integrated via a co-simulation procedure. A contact model based on a penalty formulation is selected to represent the pantograph-catenary interaction. The methodology is applied to the study of high speed train operations with multiple pantographs, as this environment constitutes one of the limiting scenarios for the increase of the operation speed.

Key words: multibody dynamics, finite elements, contact mechanics, co-simulation

1. Introduction

A limitation on the velocity of high-speed trains concerns the ability to supply the proper amount of energy required to run the engines, through the catenary-pantograph interface (Collina and Bruni, 2002). Due to the loss of contact not only the energy supply is interrupted but also arcing between the collector bow of the pantograph and the contact wire of the catenary is observed, leading to deterioration of the functional conditions of the two systems. Higher contact forces would lead to less incidents of loss of contact but would also lead to higher friction forces and, consequently, to higher wear of the catenary contact wire and pantograph registration strip (Bucca and Collina, 2009). A balance between contact force characteristics and wear of the energy collection system is the objective of improving contact quality.

The quest for higher speeds for train operations requires changes in the catenaries and pantographs in which the increase of the wave travelling speed on the contact wire plays the central role, being this achieved by decreasing the weight per unit of length of the contact wire and increasing its tension (Collina and Bruni, 2002). For instance, to achieve the world record of 574.8 km/h by a French high-speed train, the contact wire used was made of copper with a cross-section of 150 mm^2 and subjected to an axial tension of 40000 N, while the voltage in the line was increased from 25 kV to 31 kV (Pupke, 2010). In order for the Sinkansen to operate at 360 km/h, in lines that were designed for an operation up to 240 km/h not only the tension of the contact wire is increased from 14600 N to 19600 N but the tension on the messenger and auxiliary wires also changed in order to maintain the total tension at 53900 N (Ikeda, 2008).

Another important aspect of the catenary design is to maintain as constant as possible the stiffness of the contact wire to transversal loading by the pantograph registration strip (Mentel, 2008; Poetsch *et al.*, 1997). Different types of catenaries exist with alternative topological arrangements. The compound catenary, commonly used in the Japanese Sinkansen, guarantees an almost uniform stiffness while maintaining the contact wire at a constant height, without

requiring pre-sag. The stitch wire catenaries, such as the French LN1 and the German Re330, use the stitch wire to improve the uniformity of stiffness around the steady-arms while in the simple catenaries, such as the French LN2 or Italian C270, the stiffness is controlled via the dropper distance around the steady-arms. For both stitch and simple catenary types there is a pre-sag of 1/1000 to further improve the uniformity of the stiffness (Poetsch *et al.*, 1997).

The overhead catenary system is a very lightly damped structure in which the damping characterization is important, in particular when the trains are equipped with multiple pantographs (Poetsch *et al.*, 1997). Different studies show that the evaluation of the pantograph-catenary contact quality is highly dependent on the amount of structural damping considered for the catenary structural elements (Ambrósio *et al.*, 2010). However, it is also recognized that the estimation of the structural damping of the catenary is still a challenge. The catenary system dynamics exhibits small displacements about the static equilibrium position being the slacking of the droppers the only nonlinearities. Therefore, the linear finite element method has all features necessary to the modeling of this type of systems, provided that the nonlinear effects are suitably modeled as nonlinear forces, in this case, the dropper slacking can be handled by adding corrective terms to the system force vector.

The aerodynamic forces due to the direct effect of the wind on the overhead contact line, direct effect on the pantograph components and indirect effect due to the additional motion of the carbody imparted to the base of the pantograph influence the dynamics of the pantograph and catenary (Kiessllng *et al.*, 2002; Poetsch *et al.*, 1997; Pombo and Ambrósio, 2012; Pombo *et al.*, 2009). Any dynamic analysis methodology that aims at addressing a realistic modeling of the pantograph must allow handling these aerodynamic loads. In any case, the problem of characterizing and controlling the pantograph aerodynamics, although addressed in several technological projects, is still an open issue for research (EUROPAC, 2008; Pombo *et al.*, 2009).

Different pantographs are currently used in train vehicles around the world. With the exception of the Sinkansen 500 series telescopic pantograph, all high-speed railway pantographs are of the two-stage type. The topology of a pantograph must address three phases of its operation: lift the pan head to contact wire height and compensation for spans with lower catenary heights; handle the displacements and frequencies associated to steady-arms passage; deal with the displacements and frequency excitations due to the dropper passage and to higher frequency excitations (Poetsch *et al.*, 1997). Typically, the pantograph head with its suspension is responsible for handling the high-frequency excitations up to 20 Hz, while the lower stage, including the pneumatic bellow, deal with the low frequency excitations, below 5 Hz. Some other effects such as the pantograph bow flexibility and aerodynamics may result in the contact force to exhibit frequency contents over 20 Hz (Collina *et al.*, 2009). Due to the range of motion of the pantograph mechanical components and to the nonlinear elements present on its construction, multibody methods are well suited to handle the pantograph dynamics (Ambrósio *et al.*, 2012; Pombo *et al.*, 2009). Special models based on the use of lumped masses can still be used in the framework of linear finite element methods (Collina and Bruni, 2002), however, the use of multibody methods ensure that both lumped mass and detailed nonlinear pantograph models can still be used in the analysis of the pantograph-catenary interaction problem. Hybrid methodologies in which the catenary dynamics is evaluated using a linear finite element model and the pantograph dynamics is obtained using a real prototype in a test bench are hardware-in-the-loop alternatives to fully computational oriented approaches (Facchinetti and Bruni, 2012).

The interaction of the pantograph and catenary is achieved through the contact of the pantograph registration strip on the catenary contact wire. The modeling of contact between the registration strip and the contact wire can be done using unilateral kinematic constraints (Seo *et al.*, 2005), which does not require the estimation of any contact law parameter but prevents the occurrence of the loss of contact. Alternatively, penalty formulations can be used (Poetsch *et al.*, 1997; Rauter *et al.*, 2007) with no limitations on how contact may develop but requiring that

the penalty terms of the contact law are estimated. In any case, the use of different methods to handle the dynamics of the catenary and pantograph requires that either a single code in which both methods are implemented is developed or that a co-simulation strategy between the two codes is implemented (Ambrósio *et al.*, 2008; Schaub and Simon, 2001). The contact modeling plays a central role in the establishment of the co-simulation strategies (Ambrósio *et al.*, 2008).

The quality of the pantograph-catenary contact required for high-speed train operations is quantified in current regulations (EN50317, 2012; EN50367, 2006). The norm EN50367 specifies the following thresholds for pantograph acceptance (EN50367, 2006)

- Mean contact force (F_m) $F_m = 0.00097v^2 + 70\,\mathrm{N}$
- Standard deviation (σ_{max}) $\sigma_{max} < 0.3F_m$
- Maximum contact force (F_{max}) $F_{max} < 350\,\mathrm{N}$
- Maximum CW uplift at steady-arm (d_{up}) $d_{up} \leqslant 120\,\mathrm{mm}$
- Maximum pantograph vertical amplitude (Δ_z) $\Delta_z \leqslant 80\,\mathrm{mm}$
- Percentage of real arcing (NQ) $NQ \leqslant 0.2\%$

A limitation of the operational speed of trains is the wave propagation velocity on the contact wire C, which is given by (Dahlberg, 2007)

$$C = \sqrt{\frac{\pi^2 EI}{\rho L^2} + \frac{F}{\rho}} \tag{1.1}$$

where F is the tension of the contact wire, ρ is the contact wire mass per length unit, EI is the beam bending stiffness and L is the beam length. For high-speed catenaries, the second term of Equation (1.1) dominates the critical speed being the first term negligible. For instance, for the catenary considered in Table 1, the term $\pi^2 EI/(\rho L^2) \approx 1.3$ while $F/\rho = 15038$, for which the critical speed is 441 km/h. When the train speeds approach the wave propagation velocity of the contact wire, the contact between the pantograph and the catenary is harder to maintain due to increase in the amplitude of catenary oscillations and bending effects. In order to avoid the deterioration of the contact quality, the current regulation imposes a limit to the train speed of $V = 0.7C$.

The methods proposed in this work are demonstrated in the framework of the application of the regulation EN50367 to the operation of multiple pantographs in high-speed trains. This application addresses one of the limiting factors in high-speed railway operation that is the need to use more than a single pantograph for current collection and the disturbance that the pantographs cause on each other dynamics that worsens the quality of the pantograph-catenary contact.

2. Catenary dynamics

High-speed railway catenaries are periodic structures that ensure the availability of electrical energy for train vehicles. Typical constructions, such as those presented in Fig. 1, include masts, serving as the support for the registration arms and messenger wire, the steady arms, which not only support the contact wire but also ensure the correct stagger, the messenger wire, the droppers, the contact wire and, eventually, the stitch wire. Both messenger and contact wires are tensioned with high axial forces to limit the sag, to guarantee the appropriate smoothness of the pantograph contact by controlling the wave traveling speed and to ensure the stagger of the contact and messenger wires.

The motion of the catenary is characterized by small rotations and small deformations, in which the only nonlinear effect is the slacking of the droppers. The axial tension on the contact, stitch and messenger wire is constant and cannot be neglected in the analysis. All catenary

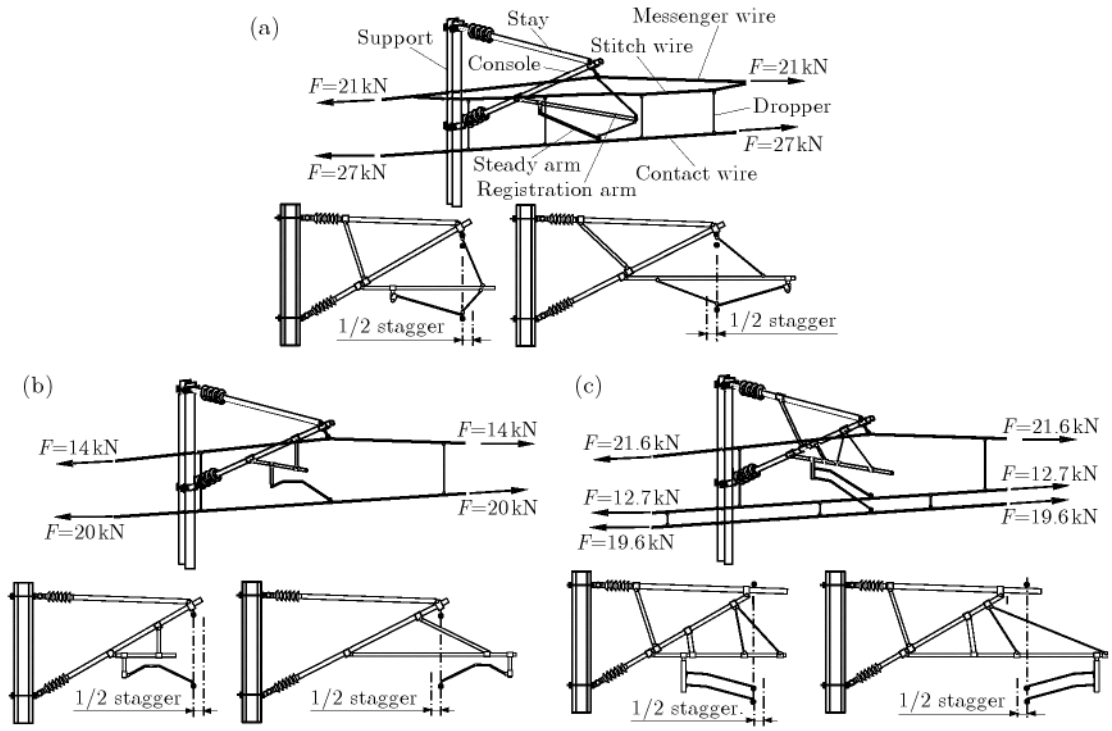

Fig. 1. Different type of high-speed catenaries implemented in the world: (a) stitch wire catenary; (b) simple catenary; (c) sinkansen catenary

elements, contact and messenger wires are modeled by using Euler-Bernoulli beam elements (Poetsch *et al.*, 1997). Due to the need to represent the high axial tension forces, the beam finite element used for the messenger, stitch and contact wire, designated as element i, is written as

$$\mathbf{K}_i^e = \mathbf{K}_L^e + F\mathbf{K}_G^e \tag{2.1}$$

in which $\mathbf{K}_L^e$ is the linear Euler-Bernoulli beam element, F is the axial tension and $\mathbf{K}_G^e$ is the element geometric matrix. The droppers and the registration and steady arms are also modeled with the same beam element but disregarding the geometric stiffening. The mass of the gramps that attach the droppers to the wires are modeled as lumped masses. To ensure the correct representation of the wave propagation 4 to 6 elements are used in between the droppers of the finite element models.

Using the finite element method, the equilibrium equations for the catenary structural system are assembled as

$$\mathbf{Ma} + \mathbf{Cv} + \mathbf{Kx} = \mathbf{f} \tag{2.2}$$

where $\mathbf{M}$, $\mathbf{C}$ and $\mathbf{K}$ are the finite element global mass, damping and stiffness matrices. Proportional damping is used to evaluate the global damping matrix, i.e, $\mathbf{C} = \alpha\mathbf{K} + \beta\mathbf{M}$ with α and β being suitable proportionality factors (Hughes, 1987), or by assembling the individual damping matrices of each finite element, i.e, $\mathbf{C}^e = \alpha^e\mathbf{K}^e + \beta^e\mathbf{M}^e$ with α^e and β^e being proportionality factors associated with each type of the catenary element, such as the dropper, messenger wire, stitch wire, etc. The nodal displacements vector is $\mathbf{x}$ while $\mathbf{v}$ is the vector of nodal velocities, $\mathbf{a}$ is the vector of nodal accelerations and f is the force vector given by

$$\mathbf{f} = \mathbf{f}_{(c)} + \mathbf{f}_{(a)} + \mathbf{f}_{(d)} \tag{2.3}$$

being $\mathbf{f}_{(c)}$ the pantograph contact forces, $\mathbf{f}_{(a)}$ the aerodynamic forces, and $\mathbf{f}_{(d)}$ the dropper slacking compensating terms.

For typical catenary finite element models, the Newmark family of integration algorithms provide suitable methods for the integration of the equations of motion (Newmark, 1959). The contact forces are evaluated for $t+\Delta t$ based on the position and velocity predictions. The finite element mesh accelerations are calculated by

$$(\mathbf{M}+\gamma\Delta t\mathbf{C}+\beta\Delta t^2\mathbf{K})\mathbf{a}_{t+\Delta t}=\mathbf{f}_{t+\Delta t}-\mathbf{C}\widetilde{\mathbf{v}}_{t+\Delta t}-\mathbf{K}\widetilde{\mathbf{d}}_{t+\Delta t} \tag{2.4}$$

Predictions for new positions and velocities of the nodal coordinates of the linear finite element model of the catenary are found as

$$\widetilde{\mathbf{d}}_{t+\Delta t}=\mathbf{d}_t+\Delta t\mathbf{v}_t+\frac{\Delta t^2}{2}(1-2\beta)\mathbf{a}_t \qquad \widetilde{\mathbf{v}}_{t+\Delta t}=\mathbf{v}_t+\Delta t(1-\gamma)\mathbf{a}_t \tag{2.5}$$

Then, with the acceleration $\mathbf{a}_{t+\Delta t}$, the positions and velocities of the finite elements at the time $t+\Delta t$ are corrected by

$$\mathbf{d}_{t+\Delta t}=\widetilde{\mathbf{d}}_{t+\Delta t}+\beta\Delta t^2\mathbf{a}_{t+\Delta t} \qquad \mathbf{v}_{t+\Delta t}=\widetilde{\mathbf{v}}_{t+\Delta t}+\gamma\Delta t\mathbf{a}_{t+\Delta t} \tag{2.6}$$

The droppers slacking is also corrected in each time step, if necessary. Although the droppers perform as bars during extension, their stiffness during compression is either null or about 1/100 of the extension stiffness, to represent a residual resistance in buckling at high speeds. As the droppers stiffness is included in the stiffness matrix $\mathbf{K}$ as a bar element anytime one of them is compressed, such contribution for the catenary stiffness has to be removed, or modified. In order to keep the dynamic analysis linear the strategy is to compensate the contribution to the stiffness matrix by adding a force to the vector $\mathbf{f}$ equal to the bar compression force

$$\mathbf{f}_{(d)t+\Delta t}=\mathbf{K}^e_{dropper}\mathbf{B}\widetilde{\mathbf{d}}_{t+\Delta t} \tag{2.7}$$

where the Boolean matrix $\mathbf{B}$ simply maps the dropper element coordinates into the global nodal coordinates.

The correction procedure expressed by using Equations $(2.5)_1$ through (2.7), followed by the solution of Equation (2.4), is repeated until convergence is reached for a given time step, i.e., until $|\mathbf{d}_{t+\Delta t}-\widetilde{\mathbf{d}}_{t+\Delta t}|<\varepsilon_d$ and $|\mathbf{v}_{t+\Delta t}-\widetilde{\mathbf{v}}_{t+\Delta t}|<\varepsilon_d$. ε_d and ε_v are user defined tolerances. Note that the criteria of convergence of the nodal displacements must imply convergence of the force vector also, i.e, the balance of the equilibrium equation right-hand side contribution of the dropper slacking compensation force with the left-hand-side product of the dropper stiffness by the nodal displacements in Equation (2.2). In practice, 6 or more iterations must be allowed in the correction process outlined.

3. Pantograph dynamics

The roof pantographs used in high-speed railway applications are characterized as mechanisms with three loops that ensure that the trajectory of the head is in a straight line, perpendicular to the plane of the base, while the pantograph heads are maintained leveled. The pantographs are always mounted in the train in a perfect vertical alignment with the center of the boggies of the vehicle in order to ensure that during curving the center of the bow does not deviate from the center of the railroad. The mechanical system that guarantees the required characteristics of the trajectory of the pantograph head during rising is generally made up by a four-bar linkage for the lower stage and another four-bar linkage for the upper stage. Another linkage between the head and the upper stage of the pantograph ensures that the bow is always leveled. In order to control the raise of the pantograph one bar of the lower four-bar linkage is actuated upon by a pneumatic actuator.

Let the configuration of the multibody system be described by n Cartesian coordinates $\mathbf{q}$, and a set of m algebraic kinematic independent holonomic constraints $\mathbf{\Phi}$ be written in a compact form as (Nikravesh, 1988)

$$\mathbf{\Phi}(\mathbf{q}, t) = \mathbf{0} \tag{3.1}$$

Differentiating Equation (3.1) with respect to time yields the velocity constraint equation. After second differentiation with respect to time the acceleration constraint equation is obtained

$$\mathbf{\Phi}_q \dot{\mathbf{q}} = \boldsymbol{\upsilon} \qquad \mathbf{\Phi}_q \ddot{\mathbf{q}} = \boldsymbol{\gamma} \tag{3.2}$$

where $\mathbf{\Phi}_q$ is the Jacobian matrix of the constraint equations, $\boldsymbol{\upsilon}$ is the right side of velocity equations, and $\boldsymbol{\gamma}$ is the right side of acceleration equations, which contains terms that are exclusively functions of velocity, position and time.

The equations of motion for a constrained multibody system (MBS) of rigid bodies, such as a pantograph, are written as

$$\mathbf{M}\ddot{\mathbf{q}} = \mathbf{g} + \mathbf{g}^{(c)} \tag{3.3}$$

where $\mathbf{M}$ is the system mass matrix, $\ddot{\mathbf{q}}$ is the vector that contains the state accelerations, $\mathbf{g}$ is the generalized force vector, which contains all external forces and moments, and $\mathbf{g}^{(c)}$ is the vector of constraint reaction equations. The joint reaction forces can be expressed in terms of the Jacobian matrix of the constraint equations and the vector of Lagrange multipliers

$$\mathbf{g}^{(c)} = -\mathbf{\Phi}_q^{\mathrm{T}} \boldsymbol{\lambda} \tag{3.4}$$

where $\boldsymbol{\lambda}$ is the vector that contains m unknown Lagrange multipliers associated with m holonomic constraints. Substitution of Equation (3.4) in Equation (3.3) yields

$$\mathbf{M}\ddot{\mathbf{q}} + \mathbf{\Phi}_q^{\mathrm{T}} \boldsymbol{\lambda} = \mathbf{g} \tag{3.5}$$

In dynamic analysis, a unique solution is obtained when the constraint equations are considered simultaneously with the differential equations of motion with the proper set of initial conditions, i.e., a set of initial conditions that fulfils the position and velocity constraint equations, described by Equations (3.1) and $(3.2)_1$, respectively. Therefore, Equation $(3.2)_2$ is appended to Equation (3.5), yielding a system of differential algebraic equations that are solved for $\ddot{\mathbf{q}}$ and $\boldsymbol{\lambda}$. This system is given by

$$\begin{bmatrix} \mathbf{M} & \mathbf{\Phi}_q^{\mathrm{T}} \\ \mathbf{\Phi}_q & \mathbf{0} \end{bmatrix} \begin{bmatrix} \ddot{\mathbf{q}}_r \\ \boldsymbol{\lambda} \end{bmatrix} = \begin{bmatrix} \mathbf{g} \\ \boldsymbol{\gamma} \end{bmatrix} \tag{3.6}$$

In each integration time step, the accelerations vector, $\ddot{\mathbf{q}}$, together with the vector of velocities, $\dot{\mathbf{q}}$, are integrated in order to obtain the system velocities and positions at the next time step. This procedure is repeated up to final time will be reached.

The solution of the multibody equations of motion and their integration in time is depicted in Fig. 2. The set of differential algebraic equations of motion, Equation (3.6)does not use explicitly the position and velocity equations associated to the kinematic constraints, Equations (3.1) and $(3.2)_1$, respectively. Thus, in order to stabilize or keep under control the constraints violation, Equation (3.6) is solved by using the Baumgarte Stabilization Method or the augmented Lagrangean formulation and the integration process is performed using a predictor–corrector algorithm with variable step and order. Due to the long simulations time typically required for pantograph-catenary interaction analysis, it is also necessary to implement constraint violations correction methods, or even the use of the coordinate partition method for such a purpose (Nikravesh, 1988).

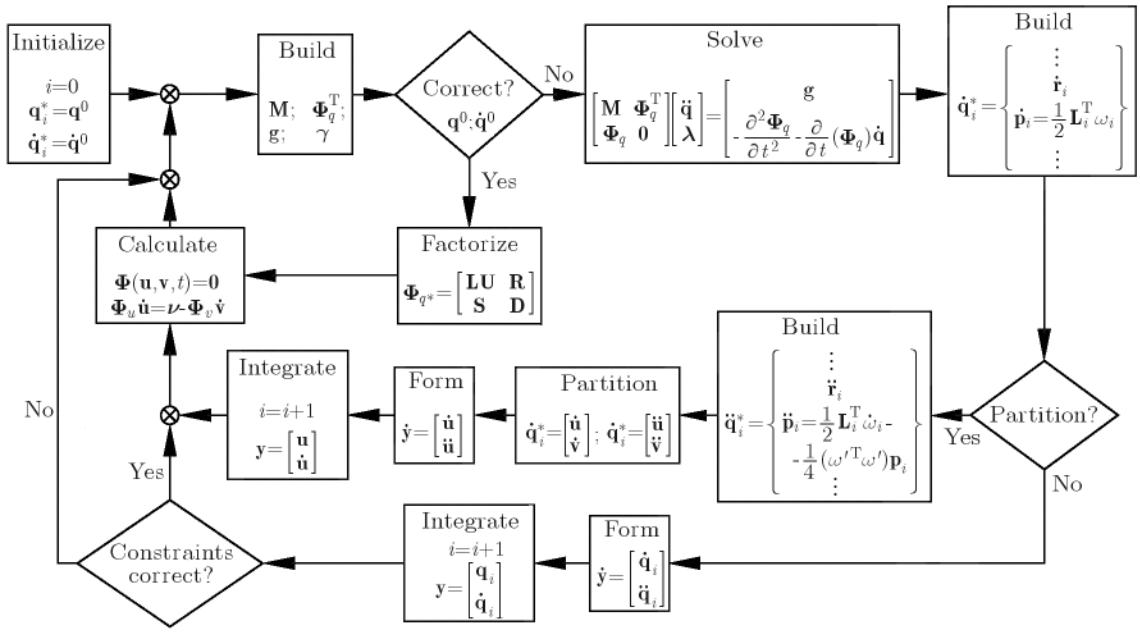

Fig. 2. Flowchart with the forward dynamic analysis of a multibody system

4. Pantograph-catenary interaction

The efficiency of the electrical current transmission and the wear of the registration strip and contact wire are highly dependent in the quality of the contact, which implies that the treatment of its contact mechanics is crucial for its correct and efficient evaluation. The contact between the registration strip of the pantograph and the contact wire of the catenary, from the contact mechanics point of view, consists in the contact of a cylinder made of copper with a flat surface made of carbon. The contact problem can be treated either by a kinematic constraint between the registration strip and the contact wire or by a penalty formulation. In the first procedure, the contact force is simply the joint reaction force of the kinematic constraint (Seo *et al.*, 2005). With the second procedure, the contact force is defined in function of the relative penetration between the two cylinders (Flores *et al.*, 2011; Pereira *et al.*, 2011). The use of the kinematic constraint between the contact wire and registration strip forces these elements to be in permanent contact. Consequently, this approach is only valid if no contact losses occur. The use of the penalty formulation allows for the loss of contact and it is the method of choice for what follows.

In this work, the Hertzian type of the contact force including internal damping is used. A suitable representation of the contact model is written as (Lankarani and Nikravesh, 1994)

$$F_N = K\delta^n\Big[1 + \frac{3(1-e^2)}{4}\frac{\dot{\delta}}{\dot{\delta}^{(-)}}\Big] \tag{4.1}$$

where the penalty term K is the generalized contact stiffness, e is the restitution coefficient, $\dot{\delta}$ is the relative penetration velocity and $\dot{\delta}^{(-)}$ is the relative impact velocity. The proportionality factor K is obtained from the Hertz contact theory as the external contact between two cylinders having their axis perpendicular to each other. Note that the contact force model depicted by Equation (4.1) is one of the different models that can be applied. Other continuous contact force models are presented by Djerassi (2012), Flores *et al.* (2011), Lee (2011). Note that the treatment of the friction forces, required for the wear predictive models, is also done with the pantograph-catenary interaction using the methodologies described by Flores *et al.* (2011). However, because these friction forces are very low, they do not influence the pantograph or catenary dynamics and, therefore, are not discussed here in further detail.

When using the same code to simulate both catenary and pantograph models the type of dynamic analysis must be the same for both, i.e., if the catenary is modeled with linear finite elements, the pantograph dynamics must also be linear. This is not compatible with the use of more general, and realistic, multibody pantograph models for which large rotations may exist or that may follow curved tracks (Pombo and Ambrósio, 2003). In order to take advantage of the more adequate type of dynamic formulations to be used for the catenary and for pantograph, a co-simulation between finite elements and multibody approaches is used here (Ambrósio *et al.*, 2008).

In a general modeling environment, in which the pantograph motion is not limited to a straight line, the analysis of the pantograph uses a multibody code while the catenary code is a finite element software. The multibody code provides the finite element code with the positions and velocities of the pantographs registration strips. The finite element code calculates the contact force, using the contact model represented by Equation (4.1), and the location of the application points in the pantographs and catenary, using geometric interference functions. The contact forces are applied to the catenary, in the finite element code, and to the pantograph model, in the multibody code, as implied in Fig. 3. Each code handles separately the equations of motion of each sub-system based on the shared force information (Ambrósio *et al.*, 2008).

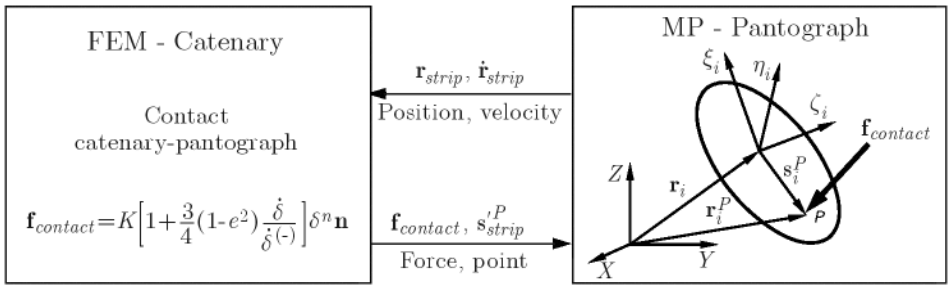

Fig. 3. Co-simulation between a finite element and a multibody code

Several strategies can be envisaged to tackle this co-simulation problem (Spiryagin *et al.*, 2012). The key of the synchronization procedure between the multibody and finite element codes is the time integration step that not only ensures the correct dynamic analysis of the pantograph-catenary system but also handles the loss and regain of contact. Let it be assumed that the finite element integration code is of the Newmark family and has a constant time step that is small enough not only to assure the stability of the integration of the catenary but also to capture the initiation of the contact between the pantograph registration strip and the contact wire of the catenary. The only restriction that is imposed in the integration algorithm of the multibody code is that its time step cannot exceed the time step of the finite element code. For a detailed description of the co-simulation procedure, the interested reader is referred to Ambrósio *et al.* (2011).

5. Pantograph-catenary case study

The numerical procedure for the dynamic analysis of the pantograph-catenary interaction is demonstrated in this work using generic, but realistic, models for the catenary and pantographs. The typical data required to build a finite element model of a simple catenary, such as that presented in Fig. 1b, is presented in Table 1.

Using the data contained in Table 1, a finite element model of the generic simple catenary is obtained. Different views of the catenary model are shown in Fig. 4. Note that in the initial and terminal spans of the catenary there is no possibility for the contact between pantograph and

Table 1. Geometric and material properties of a generic simple catenary

General			
Catenary height [m]	1.4	Contact wire height [m]	5.08
Number of spans	25	Number of droppers/span	8
N° spans at C.W. height	20	Inter-dropper distance [m]	6.75
Span length [m]	50-54	Stagger [m]	0.20
Damping α	0.0027-0.027	Damping β	0

	Contact wire	Messenger wire	Droppers	Steady arms
Material	Cu	Bz II (braided)	Bz II (braided)	–
Section [mm^2]	150	66	12	120
Mass [kg/m]	1.33	0.605	0.11	1.07
Tension [N]	20000	14000	–	–
Claw with	dropper	dropper	–	C.W.
Claw mass [kg]	0.195	0.165	–	0.200
Length [m]	–	–	1.25-1.075	1.24
Angle w/horiz.	–	–	90°	−10°

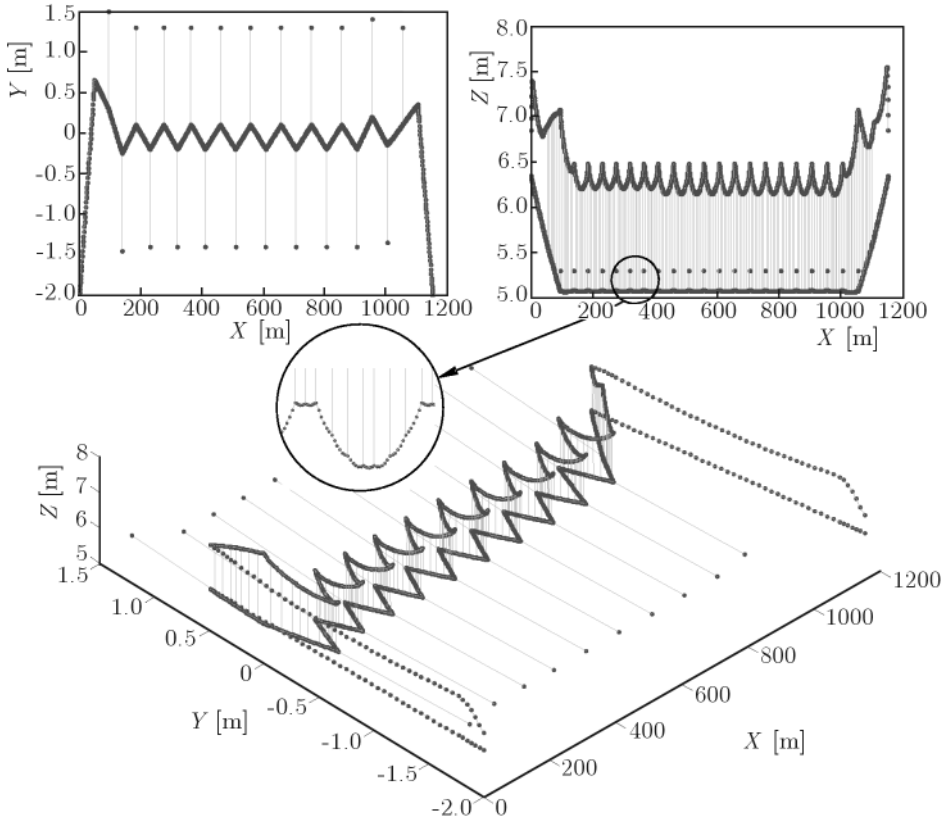

Fig. 4. Finite element model of a generic catenary with the sag highlighted

catenary to develop because in these spans the contact wire is taken away and raised from the normal position towards the tensioner devices that are used to keep the wire tension. However, the correct modeling and length of these spans is fundamental in the dynamic calculations due to the wave reflection and how it affects the pantograph-catenary interaction. Furthermore, several models of the same catenary are developed with different proportional damping factors to allow studying the variation of the pantograph-catenary contact quality in face of the structural energy

dissipation of the catenary. Note that the prediction of the catenary damping in the design phase is difficult, and only after being built, it is possible to measure it experimentally (Stickland *et al.*, 2003).

The pantograph is mounted in the roof of the vehicle as illustrated in Fig. 5. In order to establish the kinematics of the pantograph base two strategies can be used. In the first strategy, depicted by Fig. 5b the train wheelsets kinematics is guided, either by path following constraints or by the dynamics of the wheel-rail contact (Pombo and Ambrósio, 2012). The second strategy has the base of the pantograph directly guided by a path following constraint that must reflect the motion of the vehicle underneath, as seen in Fig. 5c. In what follows, the second strategy is used to guide the pantograph along a tangent track for which the catenary model has been developed.

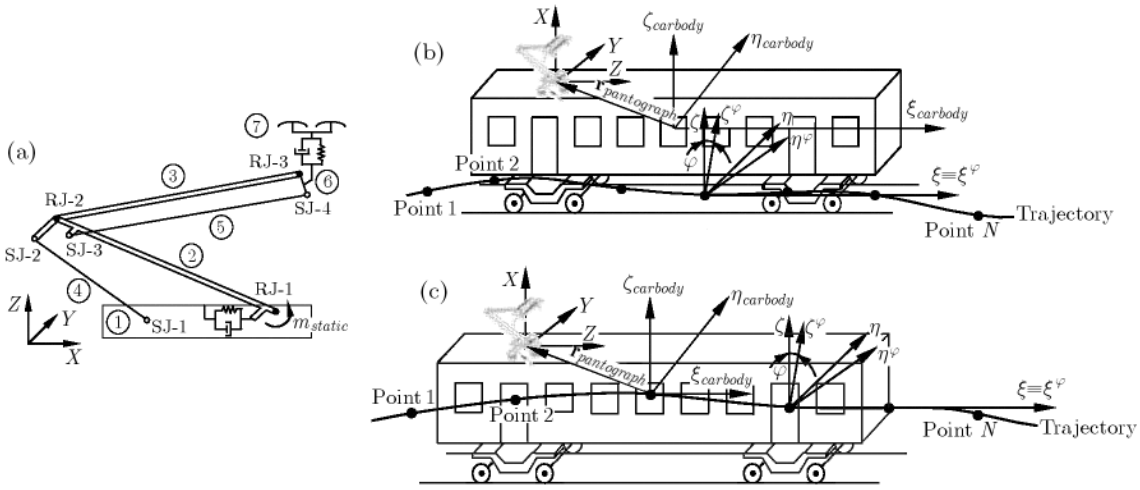

Fig. 5. (a) Pantograph model; (b) roof mounted pantograph on the vehicle guided on the track; (c) pantograph with prescribed base motion

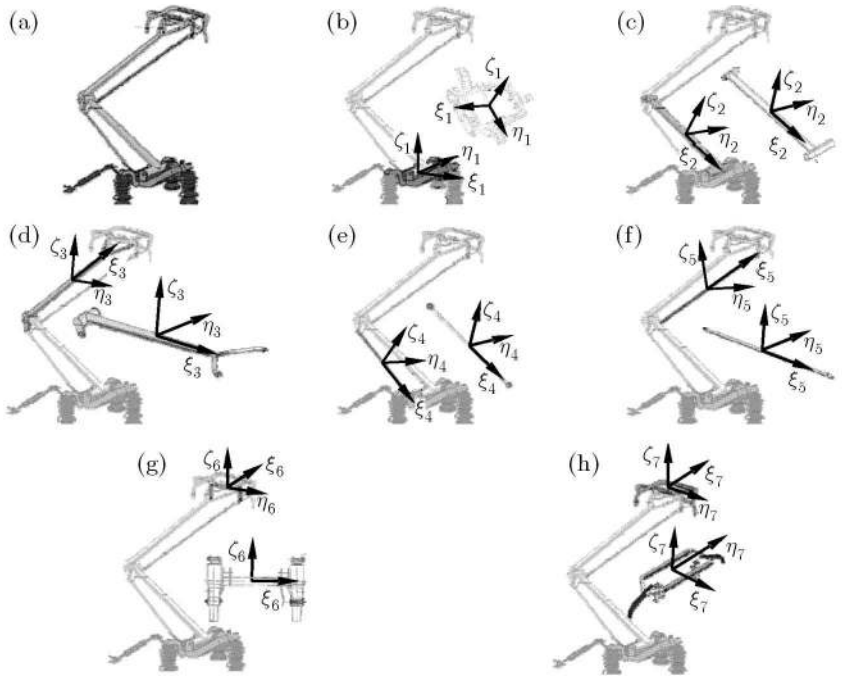

Fig. 6. The pantograph system: (a) complete pantograph; (b) base; (c) lower arm; (d) upper arm; (e) lower link; (f) upper link; (g) head support; (h) bow

The rigid bodies that compose the generic pantograph system are presented in Fig. 6. The data required for the multibody model of the pantograph concerns the mass, inertia, initial positions and initial orientations of all bodies in the system, as shown in Table 2. Note that, in this work, the data provided for the pantograph model is indicative of the configuration and properties of a particular type of generic pantograph but does not, necessarily, reflect any existing pantograph. Mechanical and constructive details such as clearance and bushing joints (Ambrósio and Verissimo, 2009; Flores *et al.*, 2011) or flexible components (Collina *et al.*, 2009) are not considered in the models presented here. However, the data gathered ensures that the dynamic performance of the model is realistic.

Table 2. Rigid body data of the pantograph multibody model

ID	Rigid body	Mass [Kg]	Inertia [Kg m^2] $I_{\xi\xi}/I_{\eta\eta}/I_{\zeta\zeta}$	Init. position [m] $x_0/y_0/z_0$	Init. orientation $e_1/e_2/e_3$
1	Panto. base	32.65	2.76/4.87/2.31	0.000/0.000/0.000	0.00/0.00/0.00
2	Lower arm	32.18	0.31/10.43/10.65	–0.571/0.000/0.412	0.00/0.17/0.00
3	Upper arm	15.60	0.15/7.76/7.86	–0.394/0.000/1.055	0.00/–0.18/0.00
4	Lower link	3.10	0.05/0.46/0.46	–0.887/0.000/0.283	0.00/0.21/0.00
5	Upper link	4.51	0.08/1.50/1.50	–0.357/0.000/1.003	0.00/–0.16/0.00
6	Stab. arm	4.67	0.34/0.01/0.50	0.553/0.000/1.418	0.00/0.00/0.00
7	Panto. head	7.80	6.62/0.23/6.87	0.553/0.000/1.498	0.00/0.00/0.00

The type and location of all kinematic joints that connect different bodies of the system, as depicted by Table 3, and the force elements characteristics, i.e., springs, dampers and actuators, must also be specified, as in Table 4. The limits of motion in the pantograph mechanical joints as well as some of the nonlinear mechanical behavior of some of the spring and damper elements are neglected in this model.

Table 3. Kinematic joints used in the pantograph multibody model

ID	Kinematic joint	Connected i	Bodies j	Attachm. points Body i $(\xi_i/\eta_i/\zeta_i)$	Local coordin. [m] Body j $(\xi_j/\eta_j/\zeta_j)$
1	Revolute joint	1	2	$(0.020/0.000/0.132)_P$ $(0.020/1.000/0.132)_Q$	$(0.820/0.000/0.000)_P$ $(0.820/1.000/0.000)_Q$
2	Revolute joint	2	3	$(–0.820/0.000/0.000)_P$ $(–0.820/1.000/0.000)_Q$	$(–1.014/0.000/0.000)_P$ $(–1.014/1.000/0.000)_Q$
3	Revolute joint	3	6	$(1.014/0.000/0.000)_P$ $(1.014/1.000/0.000)_Q$	$(0.000/0.000/0.000)_P$ $(0.000/1.000/0.000)_Q$
4	Spherical joint	1	4	$(–0.259/0.000/0.000)_P$ $(–/–/–)_Q$	$(0.688/0.000/0.000)_P$ $(–/–/–)_Q$
5	Spherical joint	3	4	$(–1.187/0.000/–0.126)_P$ $(–/–/–)_Q$	$(–0.615/0.000/–0.025)_P$ $(–/–/–)_Q$
6	Spherical joint	2	5	$(–0.780/0.000/0.000)_P$ $(–/–/–)_Q$	$(–1.000/0.000/0.000)_P$ $(–/–/–)_Q$
7	Spherical joint	5	6	$(0.962/0.000/0.000)_P$ $(–/–/–)_Q$	$(0.000/0.000/-0.105)_P$ $(–/–/–)_Q$
8	Revolute-prismatic joint	6	7	$(0.000/0.000/0.010)_P$ $(1.000/0.000/0.010)_Q$	$(0.000/0.000/0.000)_P$ $(0.000/0.000/-1.000)_Q$

A limiting factor in the current collection is the need to operate with multiple pantographs to allow for the collection of enough energy to run all the engines. However, the contact quality

Table 4. Linear force elements data used in the pantograph multibody model

ID	Force element	Stiffness [N/m]	Undef. length [m]	Damp. coeff. [N s/m]	Force [N]	Bodies i	Bodies j	Attach pts. Body i $(\xi_i/\eta_i/\zeta_i)$	Local coord [m] Body j $(\xi_j/\eta_j/\zeta_j)$
1	Sp-damp	2	0.459	60	0	1	2	(0.259/0.000/0.000)	(0.870/0.000/–0.136)
2	Actuator	0	0	0	920	1	2	(0.483/0.000/0.125)	(0.870/0.000/–0.136)
3	Sp-damp	3000	0.103	13	0	6	7	(0.000/0.335/0.000)	(0.000/0.335/0.010)
4	Sp-damp	3000	0.103	13	0	6	7	(0.000/–0.335/0.000)	(0.000/–0.335/0.010)

of the pantograph-catenary interaction is perturbed due to the mutual influence of the leading and trailing pantographs on each other. In this work, the operation of multiple pantographs in catenaries with low and moderate damping is considered. Different vehicles of high-speed trains have different lengths and, consequently, the separation distance may change accordingly. The typical separations between pantographs shown in Fig. 7 reflect how multiple train units operate and constitute the scenarios studied here.

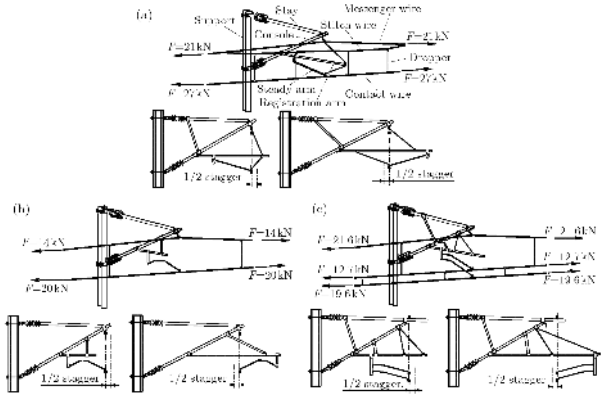

Fig. 7. Multiple pantograph operations of high-speed trains with typical distances between the pantographs

In all scenarios, the pantographs move along the catenary in a tangent track at 300 km/h. In the initial part of the analysis the pantographs are raised until their bows touch the contact wire. In order to disregard this transient part of the dynamic response, only the contact forces that develop in the pantograph between 400 and 800 m, and the droppers and steady arms that exist in this range are used in the analysis of results. The contact forces are filtered with a cut-off frequency of 20 Hz before being post-processed, as specified by the appropriate regulation (EN50317, 2012; EN50367, 2006). Figure 8 depicts the characteristics of the contact forces that develop between the pantographs and catenaries, with different proportional damping.

The results show that the amplitude of the contact forces in the trailing pantographs is always larger than what the leading pantographs exhibit, being that difference higher for lightly damped catenaries. The contact force results, as shown in Fig. 8, must be treated statistically in order to emphasize important quantities used in design and for pantograph homologation. In Fig. 9 the statistic values of the contact force are overviewed for the different pantograph separations, running in the two catenaries considered before.

The first important observation of statistical quantities depicted in Fig. 9 is that the standard deviation of the contact force for all pantographs, running on the lightly damped catenary, is always larger than 30% of the mean contact force. These values imply that the trains using these pantographs would not be allowed to run at a speed of 300 km/h in the catenary system. However, the pantographs can be used, with the current operational setup, in the catenary with normal

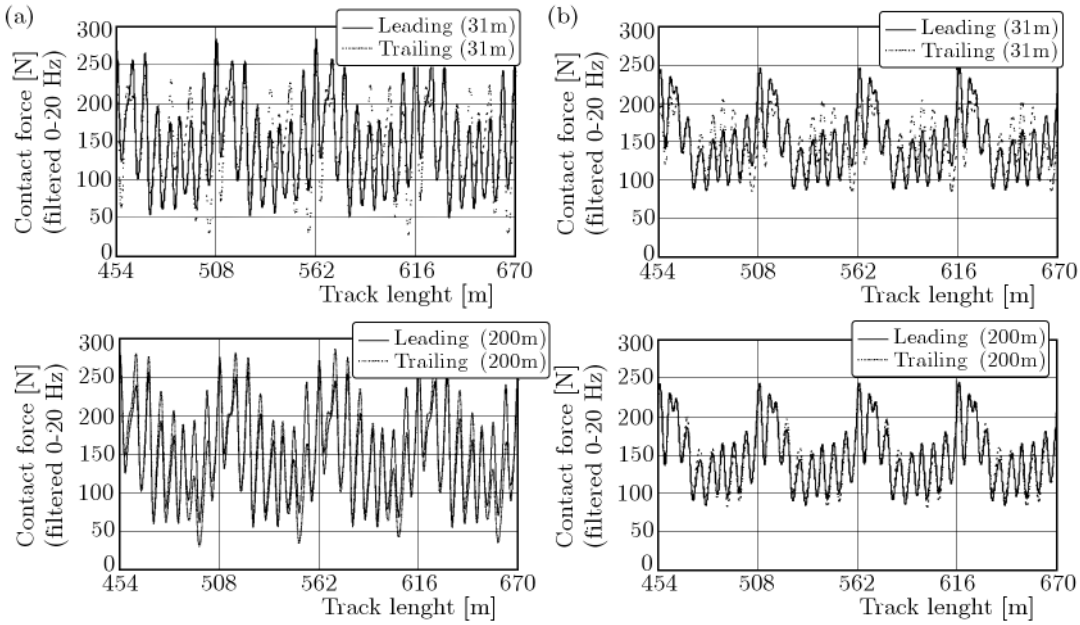

Fig. 8. Pantograph-catenary contact force for several pantograph separations in catenaries with different proportional damping: (a) $\alpha = 0.00275$; (b) $\alpha = 0.0275$

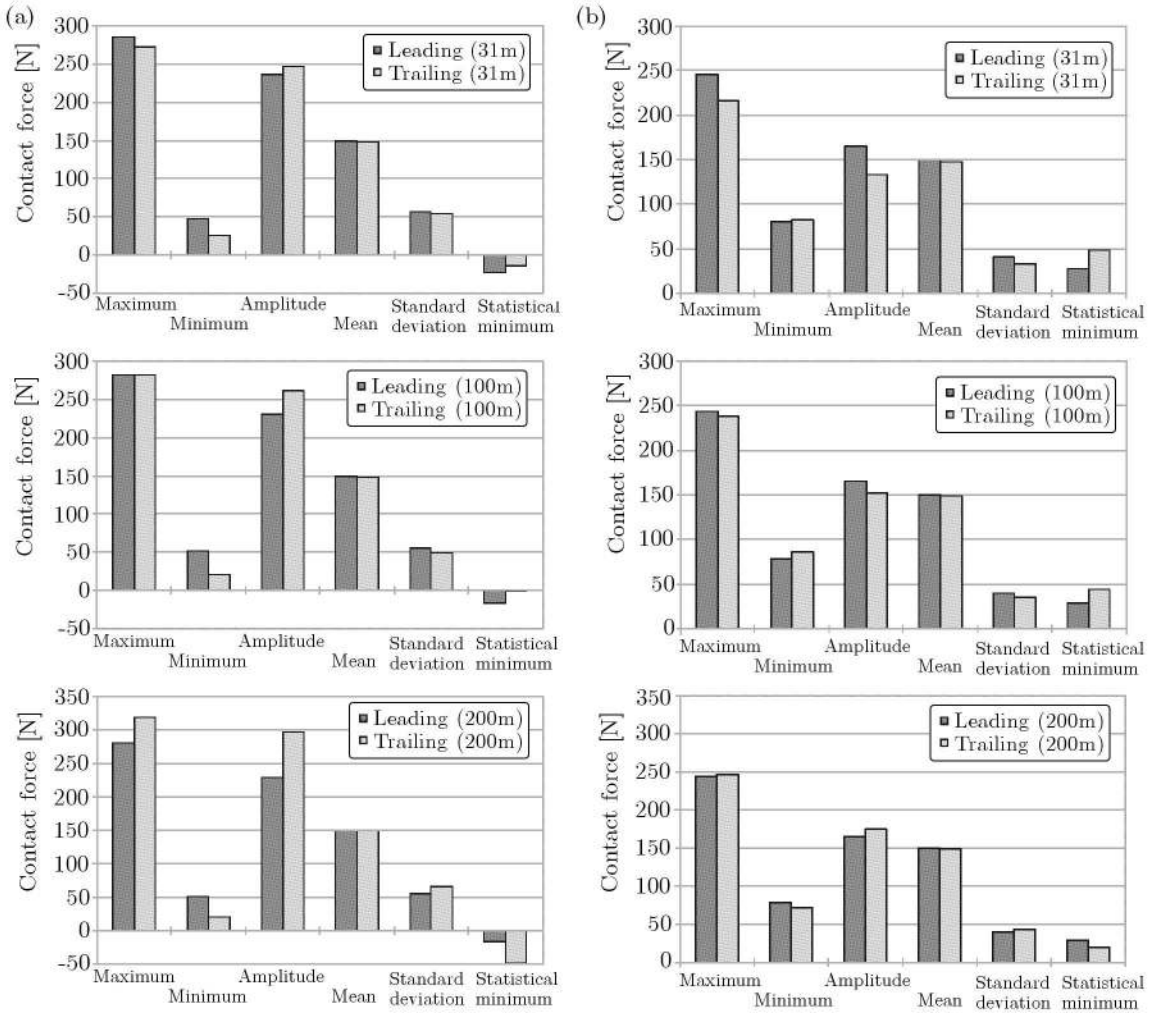

Fig. 9. Statistical quantities of the pantograph-catenary contact force in catenaries with different proportional damping: (a) $\alpha = 0.00275$; (b) $\alpha = 0.0275$

damping. In both cases, the multiple pantograph operation with a separation of 200 m shows the worst contact force characteristics for the trailing pantograph, i.e., the trailing pantograph exhibits larger maximum forces, lower minimum forces and larger standard deviations. None of the pantographs exhibits any contact loss.

Another characteristic of the contact force that is worth being analysed is its histogram. Figure 10 presents the histograms of all pantographs for all separations considered in this work. The histograms show that for a lighly damped catenary, the contact forces not only have large variations, as observed also in Fig. 8, but also that the number of occurrences of contact forces in each range considered is high, i.e., even away from the mean contact force the existence of higher or lower contact forces is not sporadic. For a catenary with average damping the contact force magnitude is closer to the mean contact force. In all cases considered, the mean contact force is always 150 N, which satisfies the regulations.

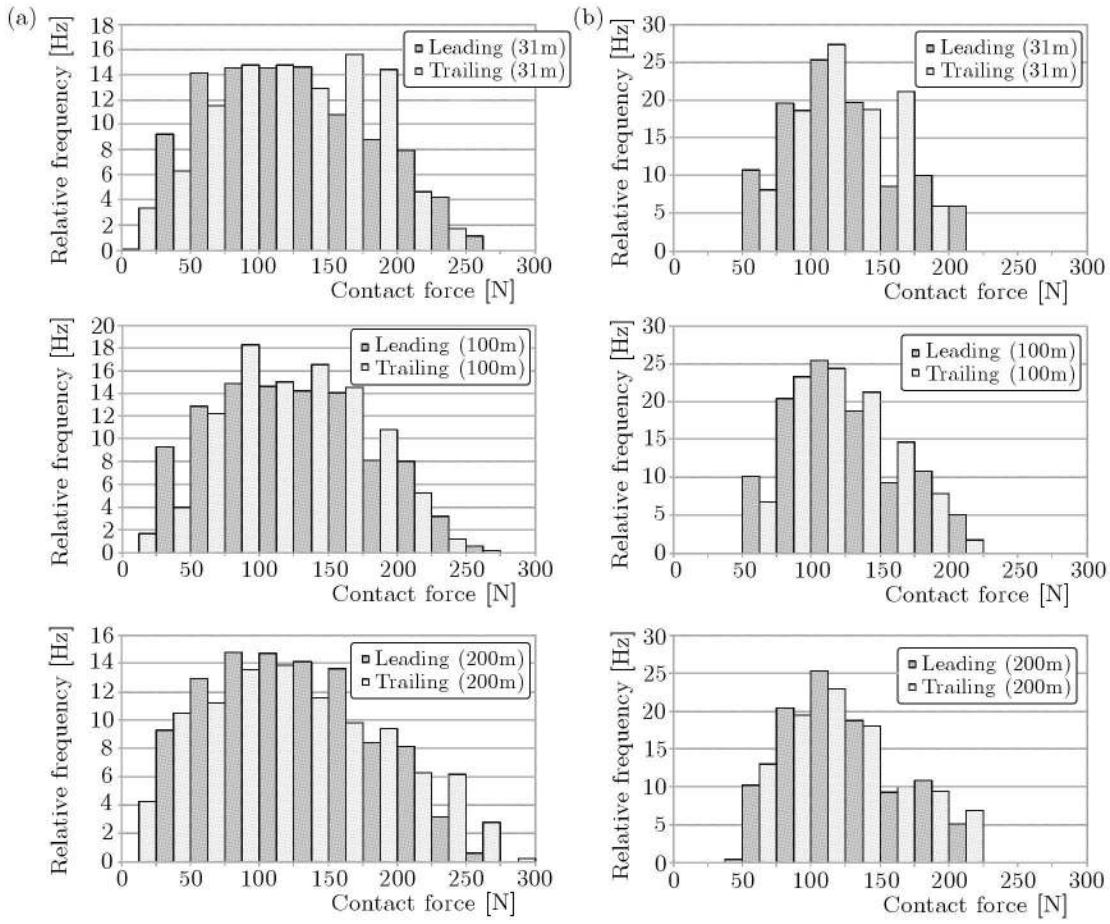

Fig. 10. Histograms of the pantograph-catenary contact force in catenaries with different proportional damping: (a) $\alpha = 0.00275$; (b) $\alpha = 0.0275$

One of the reasons why the contact force characteristics has to stay inside a limited range concerns the potential interference between the pantograph head and the catenary mechanical components. The steady-arm uplift, shown in Fig. 11, and the dropper axial force, depicted in Fig. 12, are measures of the catenary performance and of its compatibility with the running pantographs.

The steady-arm uplift is lower than 7 cm in all cases depicted in Fig. 11. Although not represented, the maximum uplift of all steady arms of the catenary is also lower than the 12 cm limit allowed for the type of catenary used. The droppers exhibit slacking for the lightly damped

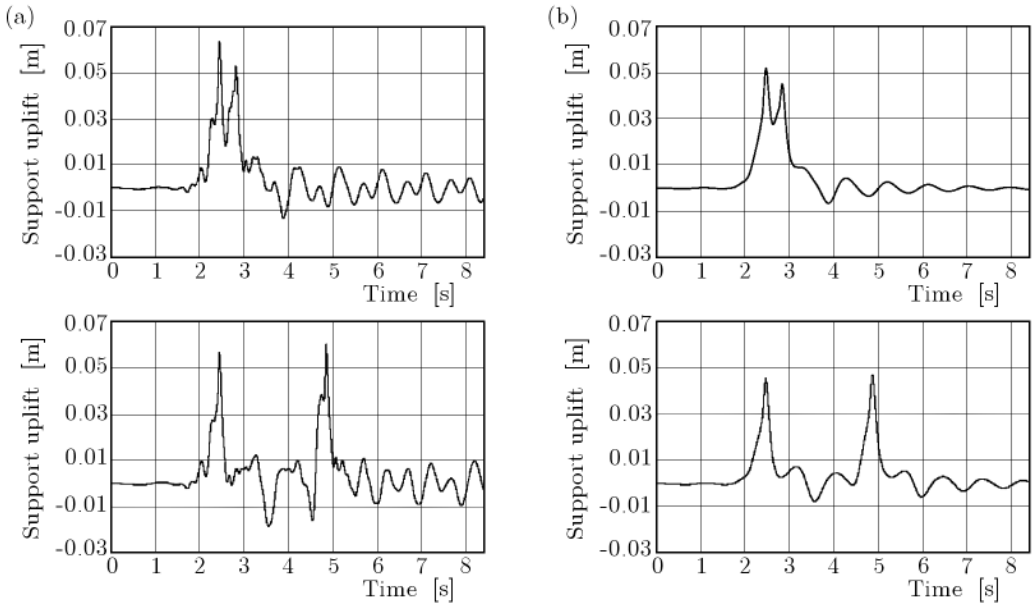

Fig. 11. Typical steady-arm uplift in catenaries with different proportional damping for two different separations of pantographs: (a) $\alpha = 0.00275$; (b) $\alpha = 0.0275$

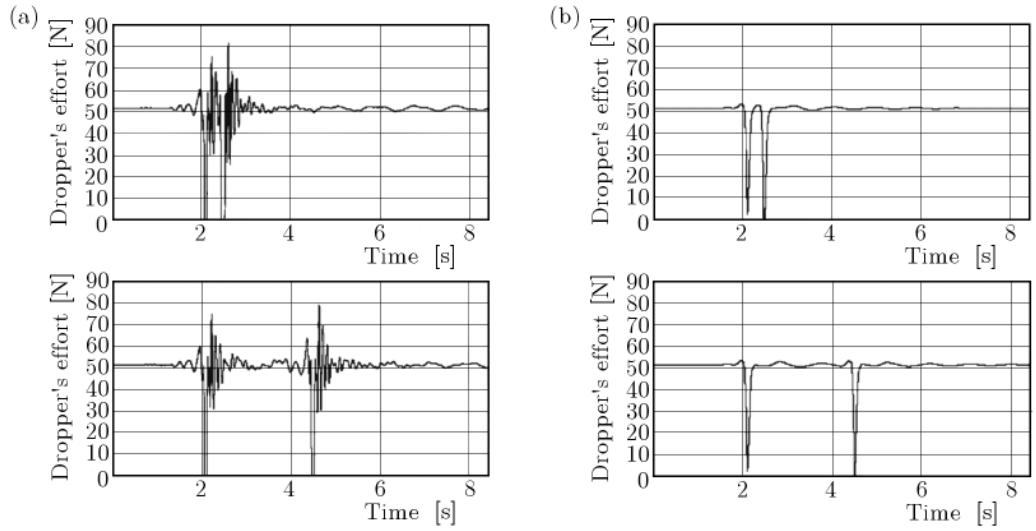

Fig. 12. Typical mid-span dropper forces in catenaries with different proportional damping for two different separations of pantographs: (a) $\alpha = 0.00275$; (b) $\alpha = 0.0275$

catenary, as seen for the axial forces shown in Fig. 12. For the catenary with average damping, only the passage of the trailing pantograph, when the separation is 200 m, has some slacking. It is interesting to notice that the position of the contact wire of the catenary is disturbed even before the pantograph bow passes. This is because the traveling wave speed is higher than the train speed. For lightly damped catenaries, this disturbance is higher. For longer catenary sections, it is expected that the trailing pantograph may affect the contact of the leading pantograph due to the wave traveling speed of the contact wire.

The mutual influence of the pantographs in each other's contact quality is better understood when displaying the contact force characteristics as shown in Fig. 13, for the lightly damped catenary and Fig. 14, for the average damped one. In both cases, the statistical values of the contact force of a single pantograph operation are also presented to better understand the problem.

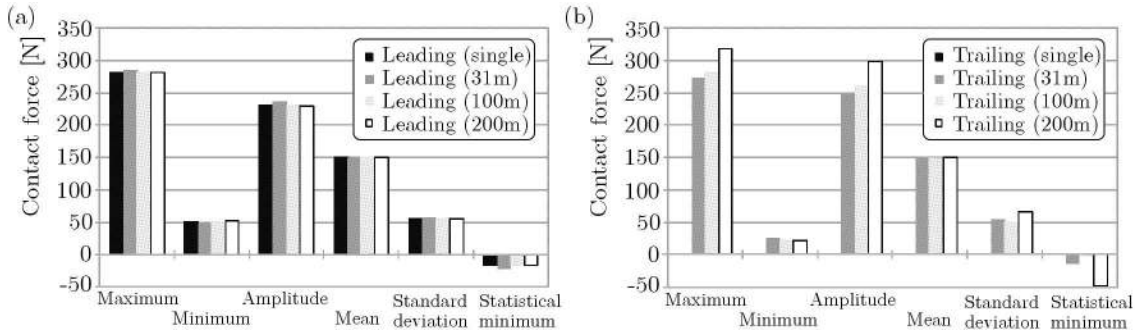

Fig. 13. Statistical quantities associated to the contact force for a catenary with low damping ($\alpha = 0.00275$): (a) leading pantographs; (b) trailing pantographs

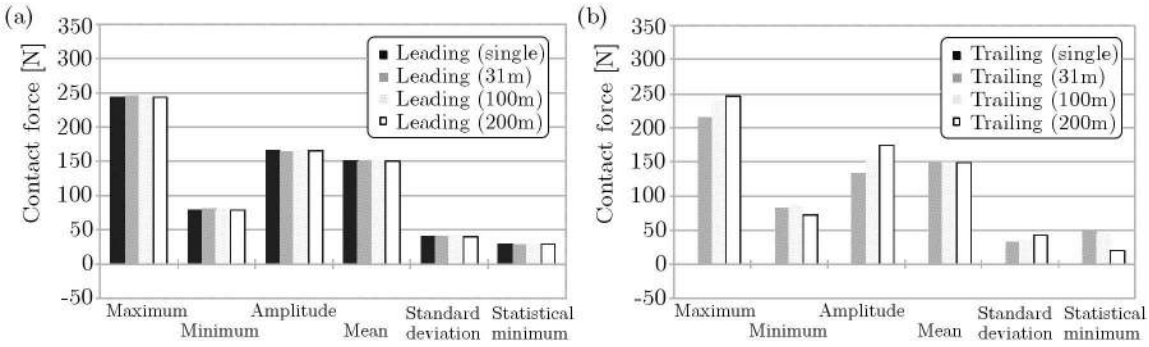

Fig. 14. Statistical quantities associated to the contact force for a catenary with average damping ($\alpha = 0.0275$): (a) leading pantographs; (b) trailing pantographs

For a lightly damped catenary, perturbations of the trailing pantograph over the leading pantograph exist but are low. However, the trailing pantograph contact forces are clearly affected by the leading pantograph, being the influence enhanced by the decrease of the catenary damping. For the lightly damped catenary with a pantograph separation of 31 m, the tendency is that the leading pantograph contact quality suffers, slightly, from the existence of a trailing pantograph. This is due to the wave traveling speed in the contact wire that is higher than the pantograph speed. For a pantograph separation of 200 m the trailing pantograph contact quality is clearly affected in both lightly and average damped catenaries. The results suggest that the critical distance between pantographs, at least for the catenary design considered in this work, is 200 m. These results are in agreement with the findings of Ikeda who studied the multiple pantograph operation for the Japanese Sinkansen pantograph-catenary interaction and found the same critical separation (Ikeda, 2008). Thus, it is suggested that regardless of the type of construction of the catenary, a critical separation distance between the pantographs exists and that the distance is close to 200 m.

6. Conclusions

A computational approach based on the co-simulation of a linear finite element and general multibody codes is presented and demonstrated in the framework of the pantograph-catenary interaction of multiple pantograph operations in high-speed trains. It was shown that linear finite elements are enough to allow the correct representation of the catenary provided that the wire tension forces are accounted for in the stiffness formulation and that the droppers slacking is properly represented via the force vector. Minimal requirements for the catenary finite element modeling include the use of Euler-Bernoulli beam elements with axial tensioning for the catenary

messenger and the contact wire with a discretization enough to capture the deformation wave traveling on the contact wire. It was also shown that the use of multibody dynamics methods allows capturing all of the important dynamic features of the pantographs. The used penalty continuous contact force model served as the vehicle for the co-simulation procedure applied.

The application of the procedures to multiple pantograph operations, in high-speed railway vehicles, allowed the identification of the important quantities of the dynamic response that are required for the pantograph homologation and for the operational decisions. The catenary damping plays a fundamental role in the pantograph-catenary contact quality. Catenary damping leads to higher maximum contact forces, lower minimum contact forces, eventually to contact losses, and to higher standard deviations of the contact forces. All these characteristics of the contact force lead to the rejection of the operation of multiple pantograph units at the required speed of 300 km/h in lightly damped catenaries. It is also concluded, from the results of the analysis, that for operations in average damped catenaries all standard separations between the pantographs lead to acceptable contact forces. As a general tendency, it was observed that for smaller pantograph separations the trailing pantograph affects the quality of the leading pantograph contact due to the wave travelling speed of the contact wire. For larger pantograph separations, it is the leading pantograph that affects adversely the contact quality of the trailing pantograph. In any case, all results show that the critical separation between the leading and trailing pantographs is 200 m, i.e., at this separation, the leading pantograph has a greater influence on the contact quality of the trailing pantograph.

Acknowledgements

The work reported here has been developed in the course of several national and international projects in which the authors have been involved. Among these, the projects SMARTRACK, funded by FCT with the contract PTDC/EME-PME/101419/2008, WEARWHEEL funded by FCT with the contract PTDC/EME-PME/115491/2009 and PANTOTRAIN, funded by the EC with the contract SC8-GA-2009-234015, resulted in important contributions. The authors want to thank Frederico Rauter, Siemens Portugal, Stefano Bruni, Alan Facchinetti and Andrea Colina, Politecnico di Milano and Jean-Pierre Massat, SNCF, whose discussions and recommendations were important to achieve some of the developments reported.

References

1. Ambrósio J., Pombo J., Facchinetti A., Bruni S., Massat J.-P., Dupuis H., 2010, Key parameters for pantograph/catenary numerical models, PantoTRAIN Technical Report D1.1, UNIFE, Brussels, Belgium
2. Ambrósio J., Pombo J., Pereira M., Antunes P., Mósca A., 2012, Recent developments in pantograph-catenary interaction modelling and analysis, *International Journal of Railway Technology*, **1**, 1, 249-278
3. Ambrósio J., Pombo J., Rauter F., Pereira M., 2008, A memory based communication in the co-simulation of multibody and finite element codes for pantograph-catenary interaction simulation, [In:] *Multibody Dynamics*, C.L. Bottasso (Ed.), Springer, Dordrecht, the Netherlands
4. Ambrósio J., Rauter F., Pombo J., Pereira M., 2011, A flexible multibody pantograph model for the analysis of the catenary-pantograph contact, [In:] *Multibody Dynamics: Computational Methods and Applications*, K. Arczewski, W. Blajer, J. Fraczek, M.K. Wojtyra (Eds.), Springer, Dordrecht, The Netherlands, 1-27
5. Ambrósio J., Verissimo P., 2009, Improved bushing models for vehicle dynamics, *Multibody System Dynamics*, **22**, 4, 341-365
6. Bucca G., Collina A., 2009, A procedure for the wear prediction of collector strip and contact wire in pantograph-catenary system, *Wear*, **266**, 1/2, 46-59

7. Collina A., Bruni S., 2002, Numerical simulation of pantograph-overhead equipment interaction, *Vehicle System Dynamics*, **38**, 4, 261-291

8. Collina A., Lo Conte A., Carnevale M., 2009, Effect of collector deformable modes in pantograph-catenary dynamic interaction, *Proceedings of the Institution of Mechanical Engineers, Part F: Journal of Rail and Rapid Transit*, **223**, 1, 1-14

9. Dahlberg T., 2007, Moving force on an axially loaded beam – with application to a railway overhead contact wire, *Vehicle System Dynamics*, **44**, 8, 631-644

10. Djerassi S., 2012, Three-dimensional, one point collision with friction, *Multibody System Dynamics*, **27**, 2, 173-195

11. EN50317 standard, 2012, Railway applications – Current collection systems – Requirements for and validation of measurements of the dynamic interaction between pantograph and overhead contact line, CENELEC European Committee for Electrotechnical Standardization, Brussels, Belgium

12. EN50367 standard, 2006, Railway applications – Current collection systems – Technical criteria for the interaction between pantograph and overhead line, CENELEC European Committee for Electrotechnical Standardization, Brussels, Belgium

13. EUROPAC, 2008, EUROPAC Publishable Final Activity Report, EUROPAC Technical Report, SNCF, Paris, France

14. Facchinetti A., Bruni S., 2012, Hardware-in-the-loop hybrid simulation of pantograph-catenary interaction, *Journal of Sound and Vibration*, DOI: 10.1016/j.jsv.2012.01.033

15. Flores P., Ambrósio J., Pimenta Claro J., Lankarani H., 2008, *Kinematics and Dynamics of Multibody Systems with Imperfect Joints: Models and Case Studies*, Springer, Dordrecht, The Netherlands

16. Flores P., Machado M., Silva M.T., Martins J.M., 2011, On the continuous contact force models for soft materials in multibody dynamics, *Multibody System Dynamics*, **25**, 3, 357-375

17. Hughes T., 1987, *The Finite Element Method: Linear Static and Dynamic Finite Element Analysis*, Prentice-Hall, Englewood-Cliffs, New Jersey

18. Ikeda K., 2008, Optimization of overhead contact lines for sinkansen speed increases, *JR East Technical Review*, **12**, 6469

19. Kiessling F., Puschmann R., Schmieder A., 2002, *Contact Lines for Electric Railways*, John Wiley & Sons Inc., Berlin, Germany

20. Lankarani H., Nikravesh P., 1994, Continuous contact force models for impact analysis in multibody systems, *Nonlinear Dynamics*, **5**, 193-207

21. Lee K., 2011, A short note for numerical analysis of dynamic contact considering impact and a very stiff spring-damper constraint on the contact point, *Multibody System Dynamics*, **26**, 4, 425-439

22. Mentel J.P., 2008, Technical developments in superstructure, *Communication at Highspeed 2008: 6th World Congress on High Speed Rail*, March 17-19, Amsterdam, The Netherlands

23. Newmark N., 1959, A method of computation for structural dynamics, *ASCE Journal of the Engineering Mechanics Division*, **85**, EM 3, 67-94

24. Nikravesh P., 1988, *Computer-Aided Analysis of Mechanical Systems*, Prentice-Hall, Englewood Cliffs, New Jersey

25. Pereira C., Ramalho A., Ambrósio J., 2011, A critical overview of internal and external cylinder contact force models, *Nonlinear Dynamics*, **63**, 4, 681-697

26. Poetsch G., Evans J., Maisinger R., Kortüm W., Baldauf W., Veitl A., Wallaschek J., 1997, Pantograph/catenary interaction and control, *Vehicle Systems Dynamics*, **28**, 159-195

27. Pombo J., Ambrósio J., 2003, General spatial curve joint for rail guided vehicles: kinematics and dynamics, *Multibody Systems Dynamics*, **9**, 237-264

28. Pombo J., Ambrósio J., 2012, An alternative method to include track irregularities in railway vehicle dynamic analysis, *Nonlinear Dynamics*, DOI 10.1007/s11071-011-0212-2, **68**, 1/2, 161-176

29. Pombo J., Ambrósio J., Pereira M., Rauter F., Collina A., Facchinetti A., 2009, Influence of the aerodynamic forces on the pantograph-catenary system for high speed trains, *Vehicle Systems Dynamics*, **47**, 11, 1327-1347

30. Pupke F., 2010, Installation of contact wire (CW) for high speed lines – recommendations, Oral presentation at IEEE Meeting, January 25, Houston, Texas

31. Rauter F., Pombo J., Ambrósio J., Chalansonnet J., Bobillot A., Seabra Pereira M., 2007, Contact model for the pantograph-catenary interaction, *JSME International Journal of System Design and Dynamics*, **1**, 3, 447-457

32. Schaub M., Simeon B., 2001, Pantograph-catenary dynamics: an analysis of models and techniques, *Mathematical and Computer Modelling of Dynamic Systems: Methods, Tools and Applications in Engineering and Related Sciences*, **7**, 2, 225-238

33. Seo J.-H., Kim S.-W., Jung I.-H., Park T.-W., Mok J.-Y., Kim Y.-G., Chai J.B., 2006, Dynamic analysis of a pantograph-catenary system using absolute nodal coordinates, *Vehicle System Dynamics*, **44**, 8, 615-630

34. Seo J.-H., Sugiyama H., Shabana A., 2005, Three-dimensional deformation analysis of the multibody pantograph/catenary systems, *Nonlinear Dynamics*, **42**, 199-215

35. Spiryagin M., Simson S., Cole C., Persson I., 2012, Co-simulation of a mechatronic system using Gensys and Simulink, *Vehicle System Dynamics*, **50**, 3, 495-507

36. Stickland M.T., Scanlon T.J., Craighead I.A., Fernandez J., 2003, An investigation into the mechanical damping characteristics of catenary contact wires and their effect on aerodynamic galloping instability, *Proceedings of the Institution of Mechanical Engineers, Part F: Journal of Rail and Rapid Transit*, **217**, 2, 63-71

Procedura obliczeniowa w analizie dynamiki układu sieci trakcyjnej i pantografu szybkobieżnego pociągu

Streszczenie

Sprawność obecnie eksploatowanych pociągów wysokich prędkości zależy od dynamicznej kompatybilności układu pantografów z siecią trakcyjną i wynikającymi siłami kontaktu pomiędzy tymi elementami. Projektowanie i analiza tego układu z wykorzystaniem odpowiednich procedur obliczeniowych pozwala uchwycić najważniejsze cechy dynamiczne obiektu badań. W pracy zaproponowano zastosowanie metody elementów skończonych do analizy dynamiki sieci energetycznej oraz równania ruchu wieloelementowego układu brył sztywnych do opisu zachowania się pantografu. Do tego celu użyto odpowiedniej procedury współsymulacyjnej. Do reprezentacji interakcji pomiędzy siecią a pantografem, wybrano sformułowanie oparte na funkcji kary. Metodologię przetestowano dla przypadku pociągów wysokich prędkości z wieloma pantografami. Ich jakość oraz jakość współpracy z siecią trakcyjną stanowi jeden z czynników ograniczających osiąganie coraz większych prędkości maksymalnych pociągów.

Manuscript received March 23, 2012; accepted for print April 27, 2012